Study of a solar photovoltaic system towards the development of an energy management algorithm

André Palminha Franco da Cruz
andrepalminha@tecnico.ulisboa.pt

Instituto Superior Técnico, Lisboa, Portugal

September 2017

Abstract

There is increasing awareness to problems related to pollution and excess energy consumption. Accompanying the new technological and scientific advances, there are new energy-efficient and non-polluting solutions that present greater savings and energetic optimization to the consumer, in an accessible and comfortable way. In the present work, an energy management tool applicable to a domestic system with photovoltaic production is proposed. The incident radiation on a panel with any orientation is studied using the Isotropic Sky, HDKR and Perez models, from horizontally incident radiation data. The modeling of photovoltaic production is achieved by using the 3-parameter model (3P), from experimental production, radiation and temperature data. The Perez and the 3P models present according results when compared to experimental data and are assembled in a toolbox of functions, which is used by a MATLAB linear programming energy management algorithm. An energy cost (in €) optimization process was simulated for a household with an integrated photovoltaic system, a thermal accumulator and a batteries system, knowing the energy consumption profiles of the occupants. The results are evaluated taking into account three different approaches: hourly and daily optimization; different initial state of charge in the batteries system; seasonal and type of day (weekday or day off) influence in the energetic consumption behavior. The daily optimization approach presents better savings when compared to the hourly one but, despite having a better overview of the whole day, is less detailed in the energy balance analysis. The initial state of charge of the batteries does not influence the optimization final result, but only the allocation of energy throughout the day. The seasonal approach results permit to conclude that in summer, the energy production exceeds the consumption and in winter, the opposite occurs, causing the system to use all the energy produced. Also from this and from the type of day approach results, it is possible to conclude that the absolute savings (in €) depend on the season and type of day, while the relative savings (in €/kWh) do not.
Keywords: Energy Management, Incident Radiation Modeling, Photovoltaic, Linear Programming, Simulations

1. Introduction

The demand for energy has been increasing for the last years and will continue to increase. It is necessary to find sustainable and environment friendly solutions to respond to the demand of energy in the world.

Renewable energy technologies are becoming more affordable and with this advent, a new paradigm is arising: the emergence and improvement of electric energy self-production systems and microgrids, which consist on small grids with a well defined boundary, that can be connected or not to the main grid.

Solar photovoltaic (PV) energy is one of the most implemented and well suited ways of electric energy self-generation for households or service, commercial or industrial buildings from a renewable source, since it can be easily personalized according to their energetic needs [1], [2].

One of the major concerns regarding these systems, is that the production depends on the availability of the sun's energy which, most of the time, may not match the needs of the consumer. There is a need of improving their efficiency not only in what regards the production, but also in what regards the consumption.

Using MATLAB, a linear programming energy management algorithm optimizes the energy cost of a case-study household, using incident radiation and PV production modeling and having the consumption profiles of its inhabbitants.

1.1. Solar Radiation

The radiation that reaches the Earth's atmosphere is different from the one that reaches its surface. The first is called extraterrestrial radiation and has a regular behavior, and the second is called terrestrial radiation and its behavior is more variable. These two types of radiation can be studied in terms of irradiance, which is the intensity of the incident solar radiation as energy per unit of time per unit of surface and of irradiation, that comes from the integration of the irradiance over a given period of time.

Generally, solar panels are tilted, with endless possible angles but most collected data corresponds to radia-

tion on a horizontal surface. The radiation that reaches a panel can be divided in its beam and diffuse components. The direction of beam radiation depends only on the geometry of the panel-sun system, while for the diffuse, it is harder to determine, since it depends significantly on the cloudiness or clearness of the atmosphere [3].

1.2. Photovoltaic Production

Solar cells are typically made of semiconductor materials, because these are good for the occurrence of the photoelectric effect. Semiconductors have the capacity of absorbing light and transmit some of its energy to electrons and holes. The separated regions (p-region and n-region) in the cell, create a well-defined electric field in the junction, thus the electrical current is generated in a preferred direction. Therefore, a PV cell may be approximated by a large scale diode [1].

In literature, there are several models that attempt to describe the best equivalent circuit for a PV cell. The most common models depend on the physical nature of the cells and on parameters relative to the characteristics of each panel (given by the manufacturer), but also depend on the weather conditions (irradiance and temperature). So, the characteristic I(V) curve of a PV cell is a non-linear equation with multiple parameters: given by the manufacturer; constant and that must be computed for certain conditions [4].

1.3. Domestic Photovoltaic Production

Having a PV or other renewable system installed in a household, it is possible to enable self-production, energy cost reduction or even energetic independence and to generate clean and sustainable energy.

There are several possible solutions to improve the efficiency of PV system and the combination with other technologies may lead to significant savings and higher efficiency.

The combination of a PV production systems with batteries solves the problem of the availability of the sun's energy. The peak of sunshine hours usually does not correspond to the periods of higher energy consumption. By having this, it allows the system to store energy instead of exporting it to the grid.

1.4. Domestic Energy Consumption Management

The study of the behavior in what regards energy consumption is a crucial part towards the implementation of energy management strategies.

There are strategies that actively implement changes in the consumers behavior, which are out of the scope of this work. The modeling of the energetic consumption will be based on fixed energetic consumption profiles.

1.5. Optimization algorithms

In literature, there can be found several optimization algorithms applied to energy management problems, but there are few examples on energy management of households with generation.

Linear programming is an optimization methodology that is used in energy management problems. It assumes that all the mathematical functions associated with a problem are linear. The decision variables x_1, x_2, ..., x_n must satisfy a system of linear equations or inequations, which translate the restrictions of the problem:

$$\sum_{k=1}^{n} a_{ik}x_k + b_i \geq 0, x_k \geq 0, i = 1, 2, ..., m \wedge k = 1, 2, ..., n \tag{1}$$

where a_{ik} and b_i are constant coefficients, n is the number of decision variables and m is the number of constraints.

The objective function tanslates what is pretended to be optimized (minimized or maximized) and is be enounced as a function of the decision variables:

$$F(x_1, x_2, ..., x_n) = c_1x_1 + c_2x_2 + ... + c_nx_n \tag{2}$$

where c_k are constant coefficients that weight the contribution of each variable [5].

2. Modeling

The modeling of the incident radiation on a panel's surface was made using the Isotropic Sky, HDKR and Perez models. For the photovoltaic production modeling, the 3 parameters model was used.

2.1. Radiation on Slopped Surfaces

Experimental data suggests that the diffuse component of solar radiation can be separated into three components: isotropic, which is uniformly distributed over the sky dome; circumsolar, which corresponds to the radiation scattered in the area in the sky around the sun; horizon brightening, which is more concentrated near the horizon [3], [6].

It is also necessary to consider the amount of radiation that is reflected by the ground and that reaches the surface, which is translated by the reflectance of the ground or albedo, ρ_g.

Adding all these components and taking into account the area of the surface, the sky, the view factor F_{a-b}, which represents the solid angle from which a can observe b and $R_b = \frac{cos\theta}{cos\theta_z}$, which the ratio between beam radiation on a tilted and on a horizontal surface, the total radiation I_T reaching a surface with any given orientation is given by:

$$I_T = I_bR_b + I_{d,iso}F_{c-s} + I_{d,cs}R_b + I_{d,hz}F_{c-hz} + I\rho_gF_{c-g} \tag{3}$$

The Isotropic Sky model assumes that the diffuse component of radiation is isotropic, *i.e*, it does not depend on the surface orientation (the tilt angle is denoted by β). From equation 3, it becomes:

$$I_T = I_b R_b + I_d \left(\frac{1+\cos\beta}{2}\right) + I\rho_g \left(\frac{1-\cos\beta}{2}\right) \quad (4)$$

The HDKR model assumes that the circumsolar component has the same direction as beam radiation and that the rest of the diffuse radiation can be split into isotropic and horizon brightening. The isotropic component is the same as in the Isotropic Sky Model and the horizon brightening uses a geometric correlation factor $\sqrt{I_b/I}\sin^3(\beta/2)$, where $\sqrt{I_b/I}$ is the term that takes into account cloudiness. From equation 3:

$$I_T = (I_b + I_d A_i) R_b + I_d (1 - A_i) \left(\frac{1+\cos\beta}{2}\right) \left[1 + \sqrt{\frac{I_b}{I}} \sin^3\left(\frac{\beta}{2}\right)\right] + I\rho_g \left(\frac{1-\cos\beta}{2}\right) \quad (5)$$

where $A_i = I_b/I_0$ is the anisotropy index and gives the fraction of diffuse radiation that has the same direction as the beam component.

The Perez model settles on a more detailed study of the three diffuse components. For this, equation 3 becomes:

$$I_T = I_b R_b + I_d (1 - F_1) \left(\frac{1+\cos\beta}{2}\right) + I_d F_1 \frac{a}{b} + I_d F_2 \sin\beta + I\rho_g \left(\frac{1-\cos\beta}{2}\right) \quad (6)$$

where F_1 and F_2 correspond to the circumsolar and horizon brightening coefficients, respectively and $a = \max(0, \cos\theta)$ and $b = \max(\cos 85^o, \cos\theta_z)$ are terms that take into account the angles of incidence of the cone of circumsolar radiation on the tilted and horizontal surfaces, respectively. F_1 and F_2 depend on the zenith angle θ_z, the brightness Δ and the clearness ϵ, that describe sky conditions.

2.2. 3 Parameters Model

The simplest model to describe a PV cell is called the Ideal Single Diode Model or the 3 Parameters Model (3P Model), which consists on a current source connected in parallel to a diode (in figure 1). The model does not take into account internal losses [4].

The output DC power of the module depends on the output voltage (V) and output current (I) by the Joule law: $P = VI$. For the 3P model [23]——, this becomes:

$$P = V\left[I_{sc} - \left(I_0\left(e^{\frac{V}{m'V_T}} - 1\right)\right)\right] \quad (7)$$

where $I_{sc} = I_s$ is the short-circuit current, I_0 is the saturation current, V_T is the thermal voltage and m' is the ideality factor, which is constant for any given conditions of temperature and irradiance and depends on V_{max}, V_T, I_{max}, I_{sc} and V_{oc}, which is the open circuit voltage.

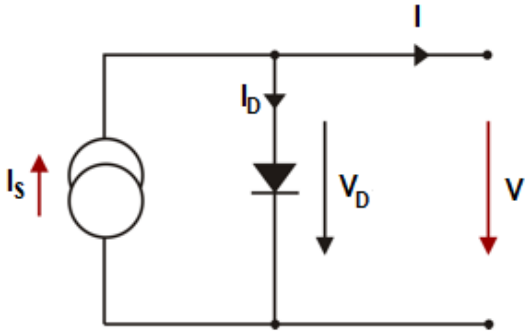

Figure 1: The Ideal Single Diode or 3P Model [27]——.

Maximum power conditions vary with temperature and irradiance. To operate continuously in maximum power, the PV modules and panels are equipped with an electronic system called maximum power point tracker (MPPT) that adjusts the output voltage, in order for the module to always work at the maximum power point (MPP). It is reached when $dP/dV = 0$. From equation 7, an equation that can be solved numerically can be obtained:

$$e^{\frac{V_{max}}{m'V_T}} = \frac{\left(\frac{I_{sc}}{I_0} + 1\right)}{\left(1 + \frac{V_{max}}{m'V_T}\right)} \quad (8)$$

2.3. Temperature Correction

The temperature affects the performance of the PV cells, changing the properties of its constituents. The output power of the cell decreases with the increase of the temperature. In particular, V_{oc} decreases significantly and I_{sc} increases slightly with temperature. The real values for these two parameters due to the temperature effect is given [1] respectively by:

$$V_{oc}^{real} = V_{oc}\left(1 + \alpha_{V_{oc}}\left(T_c - \theta^{ref}\right)\right) \quad (9)$$

$$I_{sc}^{real} = I_{sc}\left(1 + \alpha_{I_{sc}}\left(T_c - \theta^{ref}\right)\right) \quad (10)$$

where $\alpha_{V_{oc}}$ and $\alpha_{I_{sc}}$ are the open circuit voltage and short circuit current temperature coefficients, respectively.

2.4. Radiation Absorption Correction

The PV models cover is made of glass and, for any optical material, the absorption and transmittance of radiation depends on the angle of incidence.

For a clean surface, the relative transmitance (fraction of transmited radiation when compared to normal direction), comes from the Fresnel law [3], [7]. For incidence angles $\theta \leq 80^o$, it becomes:

$$FT_B(\theta) = 1 - b_0\left(\frac{1}{\cos\theta} - 1\right) \quad (11)$$

where b_0 is caracteristic for each module. For $\theta > 80^o$, the relative transmittance becomes:

$$FT_B(\theta) = 1 - \frac{\exp\left(-\frac{\cos\theta}{a_r}\right) - \exp\left(-\frac{1}{a_r}\right)}{1 - \exp\left(-\frac{1}{a_r}\right)} \quad (12)$$

where a_r is a parameter associated with the level of dirtiness. Equation 11 and equation 12 are only valid for direct and circumsolar radiation, since these have a well-defined θ. Equation 12 does not include the effects relative to normal incidence, so it is also necessary to consider the degree of dirtiness normal to the surface $T_{B_{dirt}}(0^o)/T_{B_{clean}}(0^o)$. So, the effective beam or circumsolar component of radiation reaching the PV module is:

$$G_{eff} = G\frac{T_{B_{dirt}}(0^o)}{T_{B_{clean}}(0^o)}FT_B(\theta) \quad (13)$$

3. Household Constraints

The studied system is connected to the grid and has an associated batteries bank storage system. The electric energy is supplied by three different sources: the electric grid, the PV production system and/or the batteries bank. The loads of the system are divided as being fixed or variable. The fixed loads are assumed as a baseline for the consumption profiles and the variable loads consist on the usage of a thermal accumulator and the batteries system, which are the focus of the optimization.

3.1. Inverter

The PV panels produces direct current (DC), but most devices at households use alternate current (AC). An inverter with efficiency η_{inv} is used to convert DC current into AC current. The AC power is given by:

$$P_{AC} = \eta_{inv}P_{DC} \quad (14)$$

3.2. Thermal Accumulator

The thermal accumulator water receives energy from heating and also loses energy to the surroundings. For the domestic hot water (DHW) demands, the desired water temperature (T_{DHW}) and volume (V_{DHW}) for each hour (t) are assumed as fixed. When the water is heating, the energy balance equation [8] is given by:

$$\dot{Q}_{heat}(t) = \frac{c_{p_w}\rho_w V_{DHW}(t)(T_{DHW} - T(t))}{\eta_{heat} \times 1000 \times 3600} \quad (15)$$

The energy balance for the losses takes into account the heat loss coefficient U_{loss} and is given by:

$$\dot{Q}_{loss}(t) = U_{loss}\frac{T(t) - T_{amb}}{1000} \quad (16)$$

The temperature balance of the water inside the thermal accumulator comes from equation 15 and equation 16 and by considering the average between the replaced water from the grid and the remaining water inside the thermal accumulator:

$$T(t) = \frac{V_{DHW}(t-1)T_{grid}}{V_{total}} + \frac{(V_{total} - V_{DHW}(t-1))T(t-1)}{V_{total}} \quad (17)$$

3.3. Batteries system

The battery storage capacity (in Ah) translates the yield of the battery at a given discharge rate that would drain out the battery over a specified period of time and at a given temperature.

The lifetime of the battery depends the maintenance, ambient conditions and on how the discharge goes. The currently available energy is given by the state of charge (SOC) of the battery. The depth of discharge (DOD) is the complement of SOC and gives the capacity of the battery used in terms of the total capacity [1]. The maximum available capacity at a given instant is given by:

$$C_{av_{max}} = C_{nom}(C/20, 25^oC) \times DOD_{max} \quad (18)$$

where the C_{nom} is the nominal capacity for test conditions. The available energy is given by:

$$E_{av}(t) = (SOC(t) - (1 - DOD_{max})) \times C_{av_{max}} \times V_b \times \eta_{inv} \quad (19)$$

For the charge of the batteries, it is necessary to consider the charging efficiency η_{charge}. The necessary energy to charge the battery is given by:

$$E_{charge}(t) = (SOC(t) - (DOD_{max})) \times \frac{C_{av_{max}} \times V_b}{\eta_{inv} \times \eta_{charge}} \quad (20)$$

4. Experimental Setup

The models described in 2.1 and in 2.2 were tested using experimental data and to test the energy management algorithm.

4.1. Isotropic Sky, HDKR and Perez Models Testing

The models that estimate the intensity of the incident radiation on the panels' surface were tested using data for incident radiation on a horizontal and on a tilted surface from Laboratório Nacional de Engenharia e Geologia (LNEG).

The system is located at a latitude of $\phi = 38^o46'25''$ N, a standard of longitude $L_{st} = 0^o$ and local longitude $L_{loc} = 9^o10'9''$ W and is oriented with a fixed azimuth $\gamma = 0^o$ and a variable inclination angle $\beta = 35^o$; 40^o and 45^o. It was assumed a $\rho_g = 0.2$. No significant shadowing effects were considered.

4.2. 3P Model Testing

The 3P model was tested using data from Faculdade de Ciências da Universidade de Lisboa (FCUL). The PV system is composed by 3 rows in paralel with 23 modules each.

Radiation data from a meteorological station located nearby the system was collected for the same site and orientation of the modules and used, there being no need to resort to the models described in 2.1. Temperature data came from Estação Meteorológica Automática (EMA). EMA is located in Instituto Superior Técnico and is used by the Grupo de Previsão Numérica do Tempo (GPNT).

5. Energy Management Algorithm

The optimization algorithm minimizes the cost of energy, satisfying the constraints defined by the users. The grid tariff was set as 0.1002/kWh for $h = 0$ to $h = 8$ and $h = 22$ to $h = 24$ and of 0.1909/kWh for $h = 9$ to $h = 22$. The levelized cost of electricity (LCOE) for the PV system and for the batteries was estimated to be $LCOE_{PV} = 0.0330$/kWh and $LCOE_b = 0.3624$/kWh. For the DHW, the demand was set as being $V_{DHW} = 80$l for $h = 21$ and $h = 8$ on weekdays and $h = 10$ on days off and $T_{DHW} = 60^o$C.

Two approaches were considered: hourly and daily, with two cases each.

The hourly optimization finds, for each hour, the optimal solution for charging the thermal accumulator (t) and the batteries system (b) and has a more detailed analysis on the energy balance for each equipment. The daily optimization searches for an optimal daily solution, considering the restrictions of each hour, but having a less detailed energy balance analysis.

5.1. Algorithm A - Hourly

Algorithm A optimizes first the thermal accumulor and then the batteries system. The objective function is:

$$F_{A_t}(h) = k(h) E_{g_t}(h) + LCOE_{PV} E_{PV_t}(h) + LCOE_b E_{b_t}(h) \quad (21)$$

The bound constraints on the decision variables are:

$$0 \leq E_{g_t}(h) \leq P_c \times 1hour - E_{od}(h) \quad (22)$$

$$0 \leq E_{PV_t}(h) \leq E_{AC}(h) \quad (23)$$

$$0 \leq E_{b_t}(h) \leq E_{av_b}(h) \quad (24)$$

where $P_c = 3.45$ kVA is the contracted power, E_{od} is the energy (in kWh) used by the other devices that comes from the baseline profiles, E_{AC} is the available energy from the PV system and E_{av_b} is the currently available energy on the battery, considering its SOC.

The equality constraints are:

$$E_{g_t}(h) + E_{PV_t}(h) + E_{b_t}(h) = \min \begin{cases} P_c \times 1hour - E_{od}(h) + E_{AC}(h) + E_{av_b}(h) \\ E_{heat_t}(h) \\ P_{max_t} \times 1hour \end{cases} \quad (25)$$

where E_{heat_t} is the necessary energy (in kWh) to heat the water inside the thermal accumulator until it reaches the 60^oC and P_{max_t}=2 kW is the maximum working power of the thermal accumulator.

Following the optimization of the thermal accumulator, the algorithm optimizes the batteries system. The second objective function is:

$$F_{A_b}(h) = k(h) E_{g_b}(h) + LCOE_{PV} E_{PV_b}(h) \quad (26)$$

The bound constraints are:

$$0 \leq E_{g_b}(h) \leq P_c \times 1hour - E_{od}(h) - E_{g_t}(h) \quad (27)$$

$$0 \leq E_{PV_b}(h) \leq E_{AC}(h) - E_{PV_t}(h) \quad (28)$$

The equality constraints are:

$$E_{g_b}(h) + E_{PV_b}(h) = \min \begin{cases} P_c \times 1hour - E_{od}(h) - E_{g_t}(h) + E_{AC}(h) - \\ -E_{PV_t}(h) \\ E_{charge_b}(h) \\ E_{max_b} \end{cases} \quad (29)$$

where E_{charge_b} is the necessary energy (in kWh) to charge the batteries and $E_{max_b} = 7.56$ kWh is the batteries' maximum input of energy (in kWh)

5.2. Algorithm B - Hourly

Algorithm B is similar to Algorithm A, but optimizes the batteries system first and the thermal accumulator afterwards. The objective functions and the bound and equality constraints are similar to the ones described in 5.1, but considering this order change.

5.3. Algorithm C - Daily

The daily approach find the best overall daily solution and not the individual solution for each hour, having only one objective function:

$$F_C = \sum_{h=1}^{24} [k(h)(E_{g_t}(h) + E_{g_b}(h))] + \sum_{h=1}^{24} [LCOE_{PV}(E_{PV_t}(h) + E_{PV_b}(h))] + \sum_{h=1}^{24} [LCOE_b E_{b_t}(h)] \quad (30)$$

The bound constraints are:

$$0 \leq E_{g_t}(h) \leq P_c \times 1hour - E_{od}(h) \quad (31)$$

$$0 \leq E_{g_b}(h) \leq P_c \times 1hour - E_{od}(h) \quad (32)$$

$$0 \leq E_{PV_t}(h) \leq E_{AC}(h) \quad (33)$$

$$0 \leq E_{PV_b}(h) \leq E_{AC}(h) \quad (34)$$

$$0 \leq E_{b_t}(h) \leq E_{av_b}(h) \quad (35)$$

where E_{av_b} is the available energy of the batteries system calculated at the beginning of the day.

The inequality constraints are:

$$E_{g_t}(h) + E_{g_b}(h) \leq P_c \times 1hour - E_{od}(h) \quad (36)$$

$$E_{PV_t}(h) + E_{PV_b}(h) \leq E_{AC}(h) \quad (37)$$

$$E_{g_t}(h) + E_{PV_t}(h) + E_{b_t}(h) \leq P_{max_t} \times 1hour \quad (38)$$

$$\sum_{h=1}^{24} E_{b_t}(h) \leq E_{av_b} \quad (39)$$

And the equality constrains are defined as:

$$\sum_{h=1}^{7} [E_{g_t}(h) + E_{PV_t}(h) + E_{b_t}(h)] + \sum_{h=22}^{24} [E_{g_t}(h) + E_{PV_t}(h) + E_{b_t}(h)] = E_{h_t} \quad (40)$$

$$\sum_{h=9}^{20} [E_{g_t}(h) + E_{PV_t}(h) + E_{b_t}(h)] = E_{h_t} \quad (41)$$

$$\sum_{h=1}^{24} [E_{g_b}(h) + E_{PV_b}(h)] - \sum_{h=1}^{7} [E_{b_t}(h)] - \sum_{h=22}^{24} [E_{b_t}] = E_{charge_b} \quad (42)$$

where $E_{heat_t} = 3.72$ kWh is the necessary heat in to charge the thermal accumulator from $T = 33.3^o$ C to T_{DHW}. The value for $T = 33.3^o$ C comes from equation 15 by taking $V_{DHW} = 80$ l. E_{charge_b} is the necessary energy (in kWh) to charge the batteries at the beginning of the day.

Some constraints for Algorithm C are redundant, but necessary to define the problem.

5.4. Algorithm D - Daily

The $LCOE_b$ corresponds to the highest energy cost and since the algorithm searches for the lowest cost solution, it is much likely that that the batteries system will never be used as an energy source.

Algorithm D is similar to C, but forces the system to use the batteries. It uses the same objective function, bound, inequality and equality constraints, but has an additional equality constraint:

$$\sum_{h=1}^{7} E_{b_t}(h) + \sum_{h=9}^{20} E_{b_t}(h) + \sum_{h=22}^{24} E_{b_t}(h) = E_{av_b} \quad (43)$$

6. Results

6.1. Radiation Models Testing

The acquired data corresponds to two days of each month of the year of 2015, with acquisition rates of 2 min or 30 s, with a posterior hourly average.

The value for ρ_g was assumed to be of 0.2. This value was not determined in a rigorous way, but assuming a value within a certain range [9].

For the analysis, a typical day of Summer (25th July) and a typical Winter (21st December) day were chosen, which results are represented in figure 2 and in figure 3, respectively. For each of the cases, the panels were oriented with $\gamma = 0^o$ and $\beta = 35^o$ for Summer and $\beta = 45^o$ for Winter.

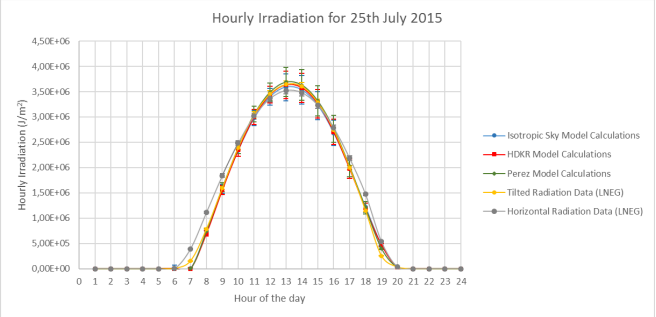

Figure 2: Hourly irradiation data and calculations for the 25th July 2015 (summer).

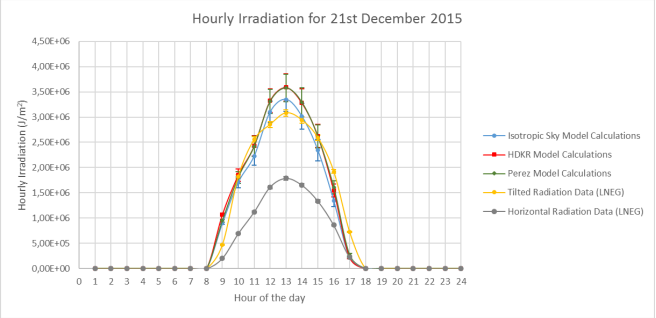

Figure 3: Hourly irradiation data and calculations for the 21st December 2015 (winter).

From figure 2, comes that the three models are very adequate. The error bars include the curve that represents the tilted surface radiation data from LNEG for each hour, except for some hours closer to sunrise and sunset.

From 3, it is possible to observe that during the period of $h = 12$ to $h = 14$, the HDKR and Perez models error bars do not include the curve for tilted surface, hence overestimating the result. However, for the remaining hours, the models are closer to the experimental result. Also, this represents a typical winter day, which can be significantly cloudy.

For periods where the values of irradiation are very low, the error is larger, since it is harder to determine the diffuse and beam components. The mean error for each model is 9.21%, 9.16% and 9.38%, respectively. The maximum experimental error is typically around

8% or 9% (with the exception of sunrise and sunset), which is close to the mean. The error might be overestimated, since the specifications of the data acquisition equipment and the characteristics of the ground were not known.

The deviation has a similar behavior to the experimental error, due to similar reasons. For the hours further from sunrise and sunset, the mean deviation is included in the maximum error and, in some cases, the error is significantly larger. The Isotropic Sky, the HDKR and the Perez models have a mean exactitude of 8.36%, 8.79% and 8.31%, respectively. Globally, the Perez model is the one that makes the better estimations.

6.2. 3P Model Testing

Representative data from one day was chosen, those days corresponding to 13th March. The data was acquired in periods of 15 minutes and afterwards averaged for each hour. The data from the system includes values of G on the plane of the panels, I_{max} and V_{max} (before the inverter).

As it was not possible to go to system's site and since it belonged to a university and not to a domestic user, it was assumed that the dirtiness degree was low, which corresponds to $T_{B_{dirt}}(0^o)/T_{B_{clean}}(0^o) = 0.98$ and $a_r = 0.20$. Also, the data for G is total irradiance for a tilted surface, thus being impossible to discriminate each component. Since this was the only available data, equation 13 was applied to the total irradiance G in order to obtain G_{eff}.

The ambient temperature T was measured in EMA in IST, which is located about 3 km away from the PV system. There are not known significant microclimate effects in the city of Lisbon so, it was assumed that the whole city would usually have the same ambient temperature.

The profile of irradiance and temperature is represented in figure 4 and the experimental and predicted values by the 3P model for I_{max}, V_{max} and P_{max} in figure 5, figure 6 and figure 7, respectively.

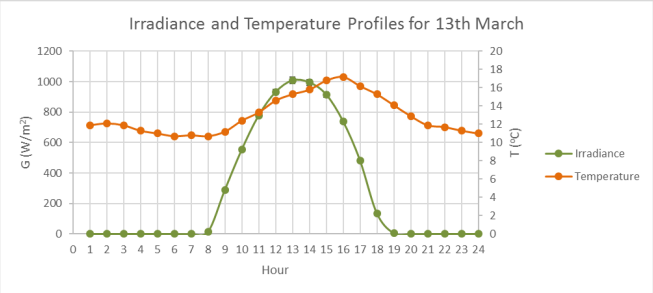

Figure 4: Mean hourly irradiance (green) and mean hourly ambient temperature (orange) for the 13th March 2015.

The profiles of I_{max} in figure 5 have a shape similar to the irradiation profile in figure 4. For the hours close to the beginning and the middle of the day, the model overestimates the value for I_{max} and the error does not include the experimental data. By the end of the day,

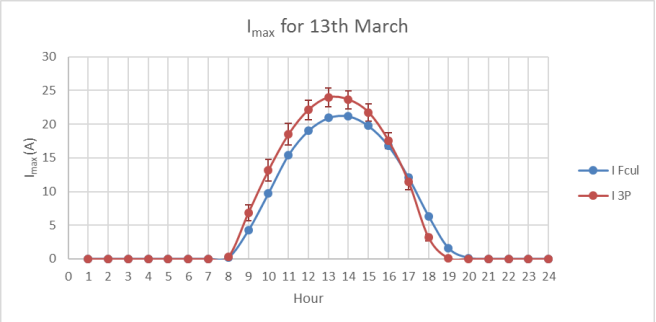

Figure 5: I_{max} experimental data (blue) and I_{max} calculations (red) for the 13th March 2015.

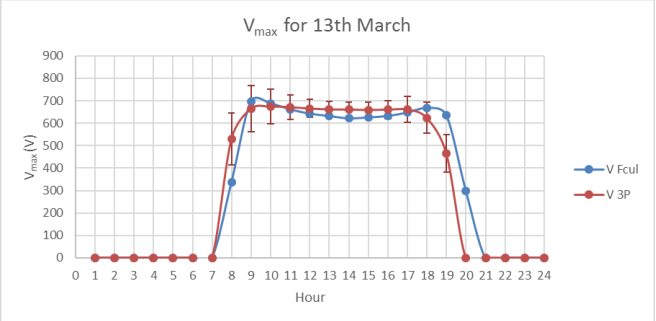

Figure 6: V_{max} experimental data (blue) and V_{max} calculations (red) for the 13th March 2015.

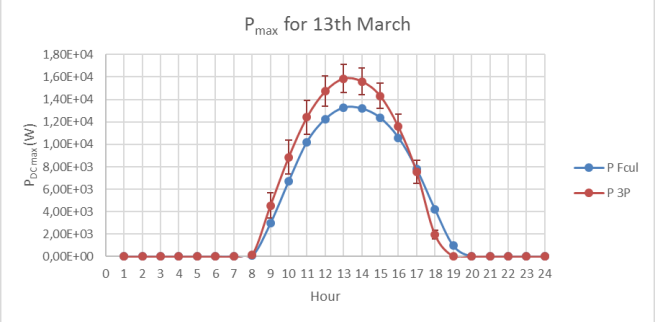

Figure 7: P_{max} experimental data (blue) and P_{max} calculations (red) for the 13th March 2015.

this inverts, being observed an underestimation of the model. Also, both curves seem to have different sunset hours.

The profiles of V_{max} have a well-defined baseline. However, this baseline presents a slight curvature on the experimental curve. The error bars include the experimental data in the baseline region of the graphic. The model also makes an overestimation at the beginning of the day and an underestimation at the end of the day.

The profiles for P_{max} in figure 7 have a shape similar to the ones of the irradiance in figure 4 and to the ones presented in figure 5. The model slightly overestimates the maximum power output of the system and the error bars, for most points, do not include the experimental curve.

For this day, the mean efficiency of the system was of $\eta = (13.91 \pm 2.15)\%$, which includes the one specified by the manufacturer of $\eta = 14.90\%$ and corresponds to

a deviation of 6.64%.

The experimental error is higher for hours closer to sunrise or sunset. I_{max} and V_{max} have mean errors of 8.40% and 9.41%, respectively and P_{max} of 11.85%. The last is higher, since it depends directly on the two previous ones. In a similar way as it was described in 6.1, the error might be slightly overestimated because, since there was no information about the equipment that measured the irradiance. The mean error of each of the three parameters appears to be reasonable and, in particular, for values closer to midday.

For the 13th of March 2015, I_{max} has a mean exactitude 16.99%, V_{max} of 9.21% and P_{max} of 20.37%. The exactitude has a similar behavior when compared with the experimental error.

G_{eff} was calculated using equation 13. All the previous calculations for the hourly values of I_{max}, V_{max} and P_{max} were repeated without using this correction. For the same day, it was obtained a mean exactitude of 21.58% for I_{max}, 9.19% for V_{max} and 25.57% for P_{max}. The usage of this correction was adequate.

6.3. Algorithm Comparison

Three different analyzes are presented: daily and hourly comparison; the influence of the initial SOC in the optimization process; the seasonal and type of day – Summer weekday and day off and Winter weekday and day off - impact. The algorithm does not use predicted values for radiation but, instead, calculations using the Perez model from data from LNEG and temperature data from EMA for the corresponding day to make the calculations.

The algorithms described in 5 were tested independently for different values of initial state of charge, $SOC_i = 40\%$, 75% and 100%. It is also assumed, that the initial temperature of the water inside the thermal accumulator is $T = 20^o$ C.

For algorithm A, in 8, the energy is allocated at the beginning of the day or immediately after the usage of the thermal accumulator. The system only charges the batteries after the thermal accumulator is optimized. Little PV energy is used, which indicates that this type of energy is might be misused or underused. The system does not take advantage of the peak of production. Results show that the batteries are already fully charged during the most intense sunshine hours. The energy used from the batteries to the thermal accumulator is very small and is only used as a backup. With this algorithm, the thermal accumulator always works at the maximum power of 2 kW (except when the water reaches the DHW temperature) and when the grid or PV limits are bellow this value, the system uses the batteries system.

The results from the hourly algorithm B are quite similar to the ones for algorithm A. By firstly powering the batteries, the available energy increases, which is afterwards used by the second optimization, where the algorithm has more available energy in the batteries to power the thermal accumulator. This is not a satisfactory result, because the optimization process is divided in two steps. The best solution would certainly be to bypass the batteries and to charge the thermal accumulator directly from the grid.

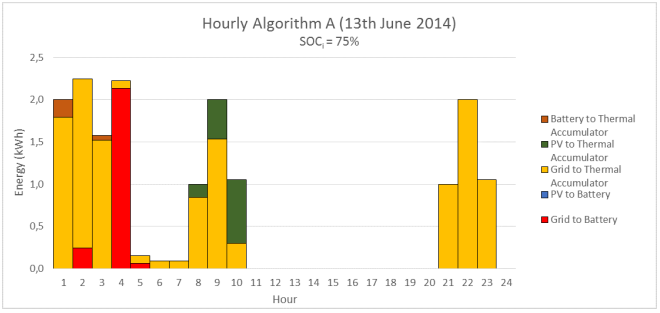

Figure 8: Hourly algorithm A results for the 13th June 2014 and $SOC_i = 75\%$.

The results from algorithm C are significantly different from the hourly ones and are shown in figure 9.

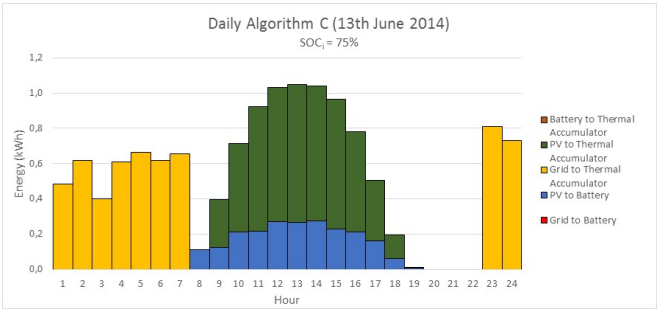

Figure 9: Daily algorithm C results for the 13th June 2014 and $SOC_i = 75\%$.

The energy is distributed throughout all day and the algorithm maximizes the usage of the PV energy. From $h = 9$ to $h = 19$, the system uses PV energy to power the thermal accumulator for the DWH demand period of $h = 20$. For the period of $h = 8$, the system recurs to the grid. The system does not power the thermal accumulator in the hours it is being used. Also, $SOC_i = 75\%$, so the battery is charged using the excess PV power, which is sufficient as the system does not recur to the grid to charge the batteries. The energy from the batteries system was not used, so the grid and PV system energy were sufficient to power the thermal accumulator.

Algorithm D presents similar results to C, but is forced to use the batteries. The batteries were used as a source but also as a load and, due to the restriction of the forced usage of the batteries, the PV production is not enough to charge the batteries throughout the day. Since this is a forced condition and the most expensive one, the algorithm distributes this usage and the system tries to maximize the charge of the batteries and minimize their usage during the sunlight hours.

To compare the different algorithms and the contribution of SOC_i, the results were assembled in the table 1.

Table 1: Comparison of the four different algorithms for 13th June with $SOC_i = 40\%$, 75% and 100%. S_t: total daily savings (in €); S: daily savings per kWh used (in €/kWh).

Different Algorithm Comparison for 13th June									
Algorithm	SOC_i	G-B	PV-B	G-T	PV-T	B-T	PV_{used}(%)	S_t(€)	S(€/kWh)
A (Hourly)	40%	5.4	0	12.4	1.4	0.2	25	0.1463	0.0925
	75%	2.4	0	12.4	1.4	0.3	25	0.1332	0.0817
	100%	0.3	0	12.4	1.4	0.3	25	0.1332	0.0817
B (Hourly)	40%	5.1	0	9.2	1.4	3.1	25	-0.6136	-0.1370
	75%	2.2	0	10.5	1.4	2.2	25	-0.3622	-0.1029
	100%	0.3	0	12.4	1.4	0.3	25	0.1332	0.0817
C (Daily)	40%	2.4	2.7	5.6	5.6	0	100	1.2910	0.1562
	75%	0	2.1	5.6	5.6	0	88.8	1.2083	0.1566
	100%	0	0	5.6	5.6	0	62.9	0.8811	0.1579
D (Daily)	40%	2.4	2.7	5.6	5.6	0	100	1.2910	0.1562
	75%	1.2	3.6	3.9	4.7	2.6	100	0.7112	0.0656
	100%	0.8	3.6	2.1	4.6	4.4	100	0.2545	0.0201

By comparing the two, it is clear that the daily approach presents better results than the hourly approach: higher savings and higher percentage of PV energy used. It is also possible to conclude that, for the daily approach, the forced usage of the battery (D) is not the ideal solution.

In the case of C, for $SOC_i = 75\%$ and 100%, there is spare PV energy, so it is possible to also sell it to the grid, which can even increase the energetic savings. The sell is also possible for A and B, but since it was not modeled, it is not possible to conclude if it would improve significantly the hourly results.

Since the C algorithm presents the best overall results, it was chosen to be used for the next optimization tests and comparisons.

6.4. Algorithm Type of Day Comparison

Algorithm C was tested for 4 different days (13th and 14th June, and 3rd and 13th December), which correspond to a typical Summer weekday and day off and Winter weekday and day off, respectively, with a $SOC_i = 75\%$. In figure 10, ir is represented the results for 3rd December.

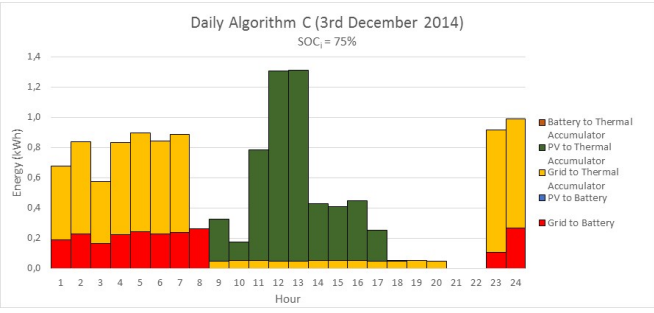

Figure 10: Daily algorithm C results for the 3rd December 2014 and $SOC_i = 75\%$.

The results for 14th July are almost equal to 13th July. But, the demand hour corresponds to $h = 10$, instead of $h = 8$, which forced the system to use the PV energy in a different way. There is also a residual use of grid energy to power the batteries, which might be due what was mentioned before.

Table 2: Comparison of the four different algorithms for typical Summer and Winter weekdays and days off with $SOC_i = 75\%$.

Different Algorithm Comparison for 13th June									
Season	Day	G-B	PV-B	G-T	PV-T	B-T	PV_{used}(%)	S_t(€)	S(€/kWh)
Summer	Week	0	2.1	5.6	5.6	0	88.9	1.2083	0.1566
	Off	0.1	2.1	5	6.2	0	100	1.2882	0.1562
Winter	Week	2.1	0	6.2	5	0	100	0.7893	0.1579
	Off	2.1	0	10.3	0.9	0	100	0.1496	0.1579

For 3rd December (figure 10), it is possible to observe the results for a typical Winter weekday. This profile also seems to maximize the usage of PV energy, but has different absolute values. The observed differences in the energy are due to the different temperature and irradiation profiles. In this case, it is interesting to observe that all of the PV energy was used to power the thermal accumulator and that it also necessary to recur to the grid as a backup.

For 13th December, most of the differences are due to the different consumption, temperature and irradiation profiles. Also, there is the difference in the DHW demand hour in the morning, which conditions the results, which lead to a small usage of the PV energy to charge the batteries at $h = 8$ and $h = 9$. The available PV energy was likely to be small for this day, which explains the low amount of PV energy used.

The results are presented in table 2.

The main difference between the seasons lies in the usage of PV energy, which is due to different seasonal sunshine hours availability. For that fact, the total savings are significantly higher in summer, but the daily savings per kWh are close. On the other hand, the differences between weekdays and days off are not relevant in Summer and in Winter are only due to the different irradiation profiles.

88, 9% of the PV energy was used in a summer weekday, which supports the idea that the system could be oversized. But, in fact, for the other three days, the system used 100% of PV energy, so the previous assumption was not necessarily correct.

7. Conclusions

The Isotropic Sky, HDKR and Perez model are adequate to convert the values for hourly irradiation on a horizontal surface to any tilted surface. Despite this, the one that presented best results, i.e., the lowest deviation from the experimental data, was the Perez model.

For the 3P model, the results were not so satisfactory. For the predictions of I_{max}, V_{max} and P_{max}, the deviation is considerably high. In spite of this, the predictions of the 3P model have a similar shape to the experimental data, but present an apparent hour displacement, which can explain the high deviation. The experimental setup was not the ideal, since the three

rows of panels are placed approximately 30 m apart and the meteorological station is placed about 100 m from the furthest row. This is relevant in what regards shading effects. On the left of the system, there is a building close enough to cast a shadow and this can effect can be noticed for the panels and for the meteorological station in different hours. Also, the temperature data was used for a location about 3 km from the experimental setup site. It was assumed that there were not considerable microclimate effects in the city of Lisbon. With the consideration, the results were compared to the predictions that did not consider this factor and presented a lower deviation, which proved that this was an adequate consideration.

The hourly approach made a more detailed optimization for the thermal accumulator and batteries energy balance for each hour, losing the scope of the whole day. It was not possible to optimize simultaneously the thermal accumulator and the batteries system, hence the development of two algorithms. Algorithm A presented positive savings, while B presented negative savings. Both algorithms presented only a 25% use of the PV energy.

The daily approach permitted to get a wider overview of the whole day but, since the thermal accumulator and the batteries models were non-linear, it was not possible to have a detailed analysis of the energy balance. Algorithm C presented higher savings comparing to the hourly ones, but it never used the batteries system as an energy source. Algorithm D also presented higher savings, but since it forced the usage of the batteries, these were lower than the ones from C.

The influence of SOC_i in the energy management process was tested using algorithm C. For the three values of SOC_i (40%, 75% and 100%), the absolute savings were different, but the savings per kWh were similar. This parameter, only influenced the allocation of the energy throughout the day.

In the case of the influence of the season and the type of day, for the four cases, the absolute savings were different, but the savings per kWh were also similar. Regardless of the season or type of day, the system almost always used 100% of the energy from PV system, so the PV system is not oversized. In a typical summer day, there is remaining energy that can be sold to the grid.

The developed algorithm permitted to prove that a detailed model for the production can be effectively used in any energy management tool, with the integration of all the three radiation models and a PV production one. It is only necessary for the system to have access to trustworthy irradiation on a horizontal surface and temperature forecasts. With a more detailed model it is possible to increase the intelligence and independence of the system. For instance, in the PV panels are movable, the system can provide an optimal hourly or daily orientation to maximize production. Or, if the production values are lower than the predictions, it can detect situations on which whether the panels need maintenance (electrical, cleaning, etc.) or if there are shading effects (e.g. a tree in front of the household that is shading the system).

The more intelligent a management algorithm is, the better are the optimization results. The algorithm relied on a linear programming tool, with only one decision variable. Besides the cost, it could be interesting for an algorithm like this to optimize other parameters like comfort or even the production. The orientation of the panels (for the case of production) or the regulation of temperature or humidity inside the house (a comfort objective) can enter the optimization. This can be further developed with more complex machine learning tools, for which the energy production and consumption profiles can be modeled instead of assumed as a baseline. Also, it could easily manage the sale of exceeding produced energy to the grid.

The more detailed analysis of the production of the PV system allows an energy management algorithm to make smarter decisions and predictions and to increase the number of decision variables to optimization process.

References

[1] A. Luque et. al. *Handbook of Photovoltaic Science and Engineering*. Chichester, West Sussex, United Kingdom, 1st ed. edition, 2011.

[2] A. Joyce et. al. A pv / t and heat pump based trigeneration system model for residential applications, 2011.

[3] J. A. Duffie et. al. *Solar Engineering of Thermal Processes*. New Jersey, United States, 4th ed. edition, 2013.

[4] H. Bellia et. al. A detailed modeling of photovoltaic module using matlab. *NRIAG J. Astron. Geophys.*, vol. 3(1):53–61, 2014.

[5] S. Dragićević et. al. Application of linear programming in energy management. *NRIAG J. Astron. Geophys.*, vol. 4(2):227–238, 2009.

[6] K. L. Coulson. *Solar and Terrestrial Radiation*. New York, United States, 1st ed. edition, 1975.

[7] A. F. Souka et. al. Determination of the optimum orientations for the double-exposure, flat-plate collector and its reflectors. *Sol. Energy*, vol. 10(4):170–174, 1966.

[8] C. Silva et al. Modeling the impact of integrating solar thermal systems and heat pumps for domestic hot water in electric systems e the case study of corvo island. *Renew Energy*, vol. 72:113–124, 2014.

[9] A. Lopes. O sobreaquecimento das cidades - causas e medidas para a mitigação da ilha de calor de lisboa. *Territorium*, vol. 15:39–52, 2009.